Structural Design of Self-thermal Methanol Steam Reforming Microreactor with Porous Combustion Reaction Support for Hydrogen Production

Tianqing Zheng[a], Wei Zhou [a] *, Xinying Li[a], Huihui You[a], Yifan Yang[a] ,Wei Yu[a],
Chenying Zhang[a], Xuyang Chu [a] *, Kwan San Hui[b], Weihua Ding[c]
[a] *Department of Mechanical & Electrical Engineering, Xiamen University, Xiamen 361005, China*
[b] *School of Mathematics, University of East Anglia, Norwich, NR4 7TJ, United Kingdom*
[c] *Rison Hi-tech Materials Company Limited, Yiwu 322000, China*

Abstract: To replace the traditional electric heating mode and increase methanol steam reforming reaction performance in hydrogen production, methanol catalytic combustion was proposed as heat-supply mode of methanol steam reforming microreactor. Moreover, the methanol catalytic combustion microreactor and self-thermal methanol steam reforming microreactor for hydrogen production were developed. Furthermore, catalytic combustion reaction supports with different structures were designed. It was found that the developed self-thermal methanol steam reforming microreactor had better reaction performance. Compared with A-type, the $\triangle T_{max}$ of C-type porous reaction support was decreased by 24.4℃ under 1.3 mL/min methanol injection rate. Moreover, methanol conversation and H_2 flow rate of the self-thermal methanol steam reforming microreactor with C-type porous reaction support were increased by 15.2% under 10 mL/h methanol-water mixture injection rate and 340 ℃ self-thermal temperature. Meanwhile, the CO selectivity was decreased by 4.1%. This work provides a new structural design of the self-thermal methanol steam reforming microreactor for hydrogen production for the fuel cell.

Keywords: Microreactor for hydrogen production; Self-thermal reaction; Porous reaction support; Thermal distribution

---

*Corresponding author. Tel.: 86-592-2188698; Fax: 86-592-2186383
E-mail address: chuxy@xmu.edu.cn (Xuyang Chu), weizhou@xmu.edu.cn (Wei Zhou).

1. Introduction

The technology of hydrogen production by methanol steam reforming microreactor was used as one of the preferred hydrogen production technologies because of its advantages, such as high hydrogen content, low cost, renewable, safe and efficient[1-5]. However, electric heating mode was used as the main heat-supply mode of the microreactor[6-7]. The high power consumption of electric heating mode limited the application of methanol steam reforming microreactor for hydrogen production in the fuel cell, especially in the mobile power station using fuel cell[8].

The solar energy, methanol combustion and butane combustion used as the heat-supply mode for methanol steam reforming microreactor for hydrogen production had been investigated by some scholars[9-13]. For example, Gu *et al.* designed and manufactured a small portable condenser collector to supply heat for the methanol reforming process for hydrogen production[9]. Chein *et al*. developed a methanol steam reforming microreactor for hydrogen production with the combustion chamber, which used methanol catalytic combustion to supply heat for methanol steam reforming for hydrogen production[10].

However, the above studies emphasized on the application of heat-supply mode in methanol steam reforming reaction. The thermal distribution of the exothermic reaction plate for different heat-supply modes has not been systematically investigated. The reaction performance of the catalyst for methanol steam reforming for hydrogen production was affected by the thermal distribution of the microreactor[6, 14]. In this way, the methanol steam reforming reaction performance in hydrogen production was

Nomenclature

Variables

m	volume proportion of CO in reaction gas, %
n	volume proportion of CO_2 in reaction gas, %
S_{co}	the selectivity of CO in reaction gas, %
V_{H2}	flow rate of H_2, mol/h
$V_{injection}$	injection velocity of the methanol-water mixture, mL/h
$V_{reaction\ gas}$	injection velocity of reaction gas, mL/min
X_{CH3OH}	methanol conversion, %
z	volume proportion of H_2 in reaction gas, %

Abbreviations

PPI	pores per inch
$\triangle T_{max}$	the maximum temperature difference of thermal distribution

related to the thermal distribution of the microreactor. Therefore, it was necessary to study the thermal distribution of the heat-supply process.

In fact, studies on the thermal distribution of exothermic reaction plate which was heat-supplied by different heat-supply technologies have been investigated by a few research groups[12-13]. For example, Hsueh *et al.* used numerical simulations to investigate the mass-transfer and heat-transfer performances of the plate-type methanol steam reforming microreactor coupled with methanol combustor. It was found that it increased the methanol steam reforming reaction performance in hydrogen production if the flow direction relationship between methanol steam reforming gas and the methanol catalytic combustion gas flow was opposite[12]. Herdem *et al.* used numerical simulations to study the thermal distribution of microchannel methanol steam reformer. They found that the methanol steam reforming reaction performance in hydrogen production can be increased using the reaction plate with reasonable thermal distribution[13].

Although some studies on the reaction performance and thermal distribution of methanol steam reforming microreactor with different heat-supply modes for hydrogen production have been carried out, the structural design and the thermal distribution optimization of the self-thermal methanol steam reforming microreactor for hydrogen production have not been systematically reported in previous studies. The reasonable thermal distribution of reaction plate was beneficial for increasing the reaction performance of the methanol steam reforming microreactor for hydrogen production. Therefore, combined with the our previous research works of the methanol steam reforming microreactor[6-7,15], to promote the industrial application of the microreactor and increase the reaction performance of the microreactor, a methanol catalytic combustion microreactor and a self-thermal methanol steam reforming microreactor for hydrogen production were firstly developed using methanol catalytic combustion as the heat-supply mode. Then, the catalytic combustion reaction supports with different structures were designed to optimize the thermal distribution. Moreover, the thermal distribution of the different reaction supports was analyzed in detail using the infrared thermal imager and temperature inspector. Furthermore, the reaction performance of the self-thermal methanol steam reforming microreactor with the different reaction supports was compared and discussed.

2. Experimental Methods

2.1 Structural design of methanol catalytic combustion microreactor

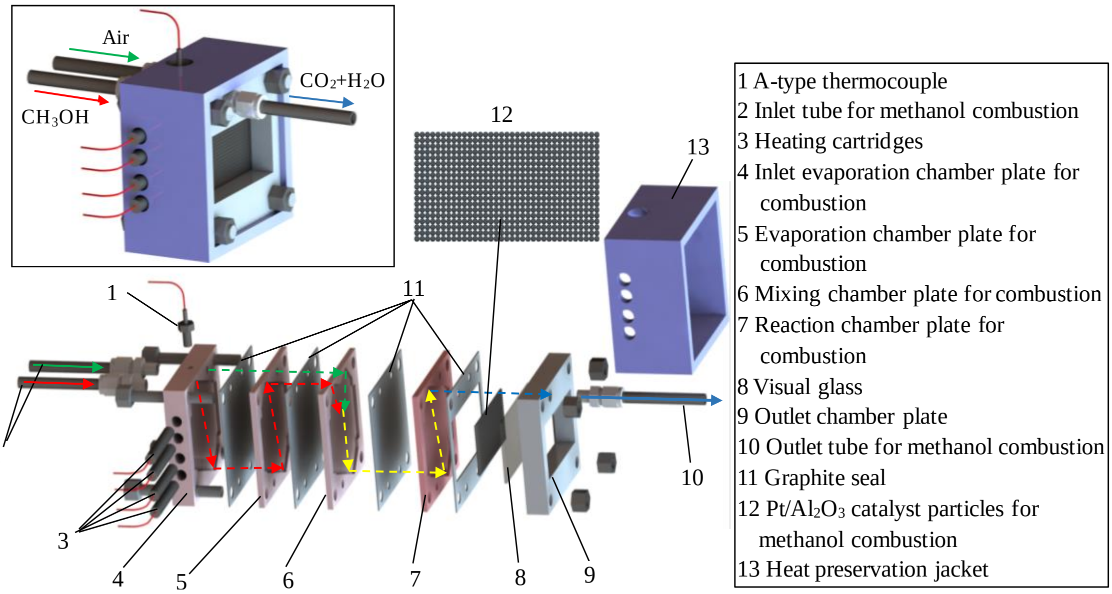

Fig.1. Structural diagram of the methanol catalytic combustion microreactor

Fig.1 shows the structural diagram of the methanol catalytic combustion microreactor. This microreactor used for combustion consisted of inlet evaporation chamber plate, evaporation chamber plate, mixing chamber plate, and reaction chamber plate for combustion; in addition, it contained a visual glass, an outlet chamber plate and a heat preservation jacket. The inlet chamber plate and evaporation chamber plate for combustion were used to convert the liquid methanol into gaseous methanol. The mixing chamber plate for combustion was used to mix methanol and air. The reaction chamber plate for combustion with a 70 mm × 40 mm × 2 mm chamber was filled with catalytic combustion reaction support. The visual glass was set in the outlet chamber plate, and it was used to observe the methanol catalytic combustion reaction in the reaction chamber plate for combustion. The heat preservation jacket was used to preserve heat in the microreactor.

Liquid methanol was gasified through the inlet evaporation chamber plate and evaporation chamber plate for combustion, and it was subsequently mixed with air in the mixing chamber plate for combustion. Then, the mixed gas was reacted with the catalyst which was in the reaction chamber plate for combustion. Eq. (1) indicates the reaction process for methanol catalytic combustion reaction[16-19].

$$CH_3OH + 1.5O_2 \rightarrow CO_2 + 2H_2O \quad \Delta H = -192.2\ KJ/mol \tag{1}$$

2.2 Construction of testing system for the methanol catalytic combustion microreactor

Fig.2 shows a structural diagram of the testing system for the methanol catalytic combustion microreactor. The testing system mainly consisted of compressed air bottle, mass flowmeter (D07-7B, Beijing Sevenstar Electronics Company, China), peristaltic pump (BT300S, Baoding Lead Fluid Company, China), microreactor, thermostat, heating cartridges, A-type thermocouple, infrared thermal imager (FLIR T440, FLIR Systems Company, USA), and temperature inspector (AT4516, Applent Instruments Company, China). Methanol was injected into the microreactor using a peristaltic pump. Air was supplied into microreactor by air bottle and mass flowmeter. The heating cartridges and A-type thermocouple on the inlet evaporation chamber plate for combustion and thermostat were used to perform the preheat of the microreactor before the heat-supply by the methanol catalytic combustion reaction for the microreactor itself. The visual glass was set in the outlet chamber plate. The thermal distribution of the reaction chamber plate for combustion was observed using infrared thermal imager. Meanwhile, the thermal distribution of reaction chamber plate for combustion can be investigated using temperature inspector to measure the temperatures of nine temperature measurement points of the outlet chamber plate.

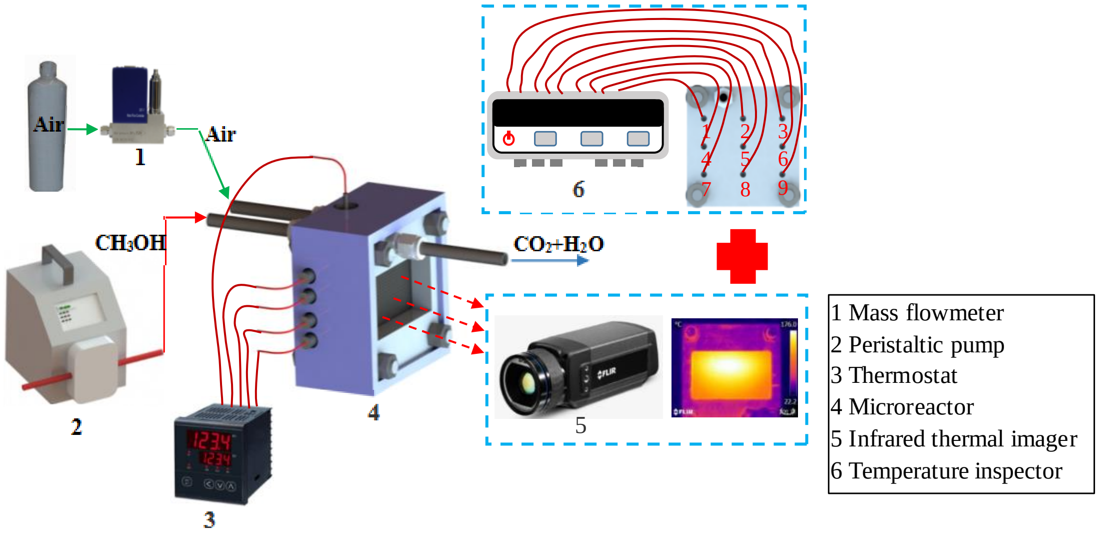

Fig.2. Structural diagram of the testing system for the methanol catalytic combustion microreactor

Before the occurrence of methanol catalytic combustion reaction, the methanol catalytic combustion microreactor was preheated by electric heating, and the heating temperature of thermostat was set to 300 °C. When the temperature on the inlet evaporation chamber plate for combustion was 300 °C, methanol and air were injected into the microreactor. Then, when the temperature on the inlet evaporation chamber plate for combustion was more than 300 °C, the heating temperature of thermostat was set to 25 °C. In this time, the methanol catalytic combustion microreactor was heat-supplied by itself. The thermal distribution on the reaction chamber plate for combustion was used as an index for evaluating the methanol catalytic combustion reaction performance of the microreactor. The methanol catalytic combustion reaction performance of the microreactor was measured using an infrared thermal imager and a temperature inspector. The infrared thermal imager was used to investigate the overall thermal distribution on the reaction chamber plate for combustion[20-21]. The temperature inspector was used to investigate the temperature differences between nine temperature measurement points on the reaction chamber plate for combustion.

2.3 Structural design of self-thermal methanol steam reforming microreactor for hydrogen production

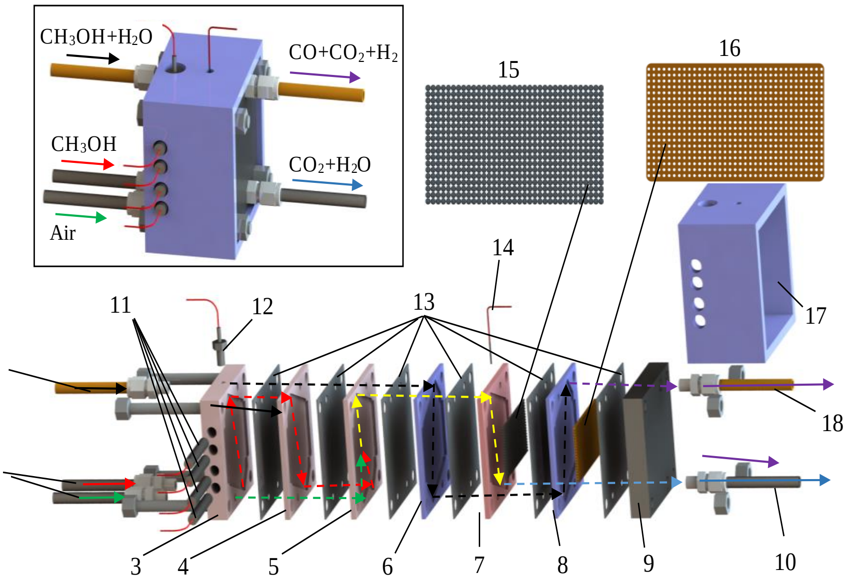

1 Inlet tube for methanol steam reforming reaction
2 Inlet tube for methanol combustion
3 Inlet evaporation chamber plate for combustion
4 Evaporation chamber plate for combustion
5 Mixing chamber plate for combustion
6 Evaporation chamber plate for reforming
7 Reaction chamber plate for combustion
8 Reaction chamber plate for reforming
9 Outlet chamber plate
10 Outlet tube for methanol combustion
11 Heating cartridges
12 A-type thermocouple
13 Graphite seal
14 B-type thermocouple
15 Pt/Al_2O_3 catalyst particles for methanol combustion
16 Copper foam loaded with Cu/Zn/Al/Zr catalyst for methanol steam reforming
17 Heat preservation jacket
18 Outlet tube for methanol steam reforming reaction

Fig.3. Structural diagram of the self-thermal methanol steam reforming microreactor for hydrogen production

Fig.3 shows a structural diagram of the self-thermal methanol steam reforming microreactor for hydrogen production. The microreactor consisted of an inlet evaporation chamber plate, evaporation chamber plate, mixing chamber, and reaction chamber plate for combustion, evaporation chamber plate and reaction chamber plate for reforming, outlet chamber plate, and heat preservation jacket. Similar to the methanol catalytic combustion microreactor, the inlet evaporation chamber plate, evaporation chamber plate, mixing chamber, reaction chamber plate and the Pt/Al_2O_3 catalyst particles were used in the methanol catalytic combustion reaction for combustion[16-19]. The methanol catalytic combustion reaction in the reaction chamber plate for combustion was used to supply heat to the reaction chamber plate for methanol steam reforming reaction. The flow direction relationship of reaction gas between the reaction chamber plate for combustion and the reaction chamber plate for reforming was opposite. The methanol for reforming was evaporated in the evaporation chamber plate for reforming. The methanol steam reforming gas was reacted with Cu/Zn/Al/Zr catalyst loaded on the copper foam in the reaction chamber plate for reforming[6,7]. The heat preservation jacket was used to preserve heat in the microreactor.

$$CH_3OH + H_2O \rightarrow 3H_2 + CO_2 \quad \Delta H = +49.4\ KJ/mol \tag{2}$$

$$CH_3OH \rightarrow CO + 2H_2 \quad \Delta H = +92.0 KJ/mol \tag{3}$$

$$CO + H_2O \rightarrow CO_2 + H_2 \quad \Delta H = -41.1 KJ/mol \tag{4}$$

The main reaction process of methanol steam reforming in hydrogen production is shown in Eqs. (2)-(4)[22-24]. Eq. (2) is the algebraic summation of Eqs. (3) and (4). Eq. (3) indicates the methanol decomposition. Eq. (4) indicates a water–gas shift reaction. The dominant products in the reaction gas are H_2 and CO_2, while a small percentage of CO exists.

2.4 Construction of testing system for self-thermal methanol steam reforming microreactor for hydrogen production

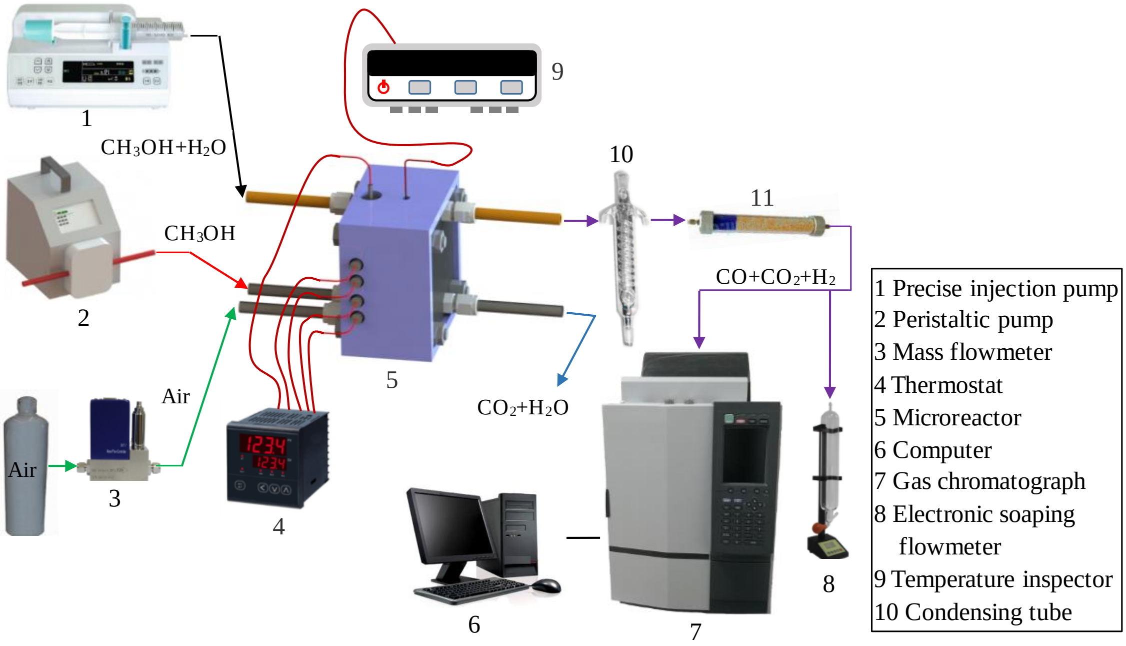

Fig.4. Structural diagram of the testing system of the self-thermal methanol steam reforming microreactor for hydrogen production

Fig.4 shows the structural diagram of the testing system of the self-thermal methanol steam reforming microreactor for hydrogen production. The testing system consisted of compressed air bottle, mass flowmeter, peristaltic pump, precise injection pump (JZB-1800, Jianyuan Medical Equipment Company, China), microreactor, thermostat, heating cartridges, A-type thermocouple, infrared thermal imager, and temperature inspector, electronic soaping flowmeter (JCL-2010(S)-A, Qingdao Juchuang Environmental Company, China), and a gas chromatograph (GC2014C with TCD and TDX-01, Shimadzu Company, Japan). The methanol-water mixture for reforming was injected into the microreactor by an injection pump. The methanol for combustion was injected into microreactor by a peristaltic pump, and air for combustion was transported into microreactor by air bottle and mass flowmeter. The temperature of the reaction chamber plate for combustion was monitored by the temperature inspector. The reaction temperature of methanol steam reforming reaction was determined by the temperature of the reaction chamber plate for combustion. The temperature of the reaction chamber plate for combustion was controlled by the flow rate of the methanol and air for combustion. The unreacted methanol and water in the methanol steam reforming gas were separated using the condensation and the drying pipes. The flow rate of reaction gas was analyzed by a soap flowmeter. The volume proportions of CO, CO_2, and H_2 in the reaction gas were determined by a gas chromatograph.

After the occurrence of the catalytic combustion reaction in the self-thermal methanol steam reforming microreactor, the methanol-water mixture was injected into the microreactor. Then, the methanol steam reforming reaction for hydrogen production was occurred in the microreactor. The methanol conversion, H_2 flow rate and CO selectivity were used as indices for evaluating the methanol steam reforming reaction performance of the microreactor for hydrogen production. Eqs. (5), (6) and (7) are the empirical formulas for calculating methanol conversion and H_2 flow rate and CO selectivity[6,7,25].

$$X_{CH_3OH}=\frac{V_{\text{reaction gas}}*(m+n)}{V_{injection}*\frac{1}{60}*\frac{1}{64}*\frac{273}{K}*22400} \tag{5}$$

$$V_{H_2}=\frac{V_{\text{reaction }gas}*\mathrm{z}}{22400*60} \tag{6}$$

$$S_{\text{co}}=\frac{m}{m+n}\times 100\% \tag{7}$$

2.5 Structural design and reaction performance investigation of porous reaction support for methanol catalytic combustion

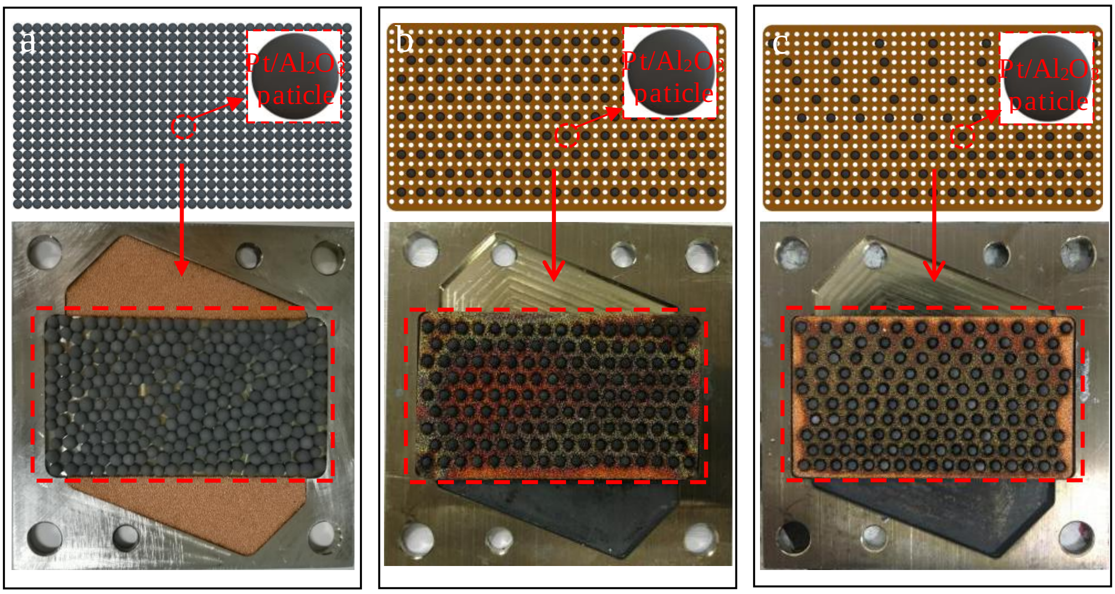

Fig.5. Structural diagram of porous reaction supports with different structural designs: (a) A-type; (b) B-type; (c) C-type structures

Fig.5 shows the structural diagram of porous reaction supports with different structural designs. Here, Pt/Al_2O_3 spherical catalyst particles with 2 mm external diameter and 1% Pt content were used. A rectangular chamber filled with Pt/Al_2O_3 catalyst particles and two oblique chambers filled with 110 PPI copper foam in the reaction chamber plate for combustion were used as catalytic combustion reaction support with A-type structure. The rectangular chamber filled with 110 PPI copper foam and the Pt/Al_2O_3 catalyst particles, which were on the 110 PPI copper foam, in uniform gap distribution, were used as catalytic combustion reaction support with B-type structure. The rectangular chamber filled with 110 PPI copper foam and the Pt/Al_2O_3 catalyst particles, which were on the 110 PPI copper foam, in gradient gap distribution were used as catalytic combustion reaction support with C-type structure.

The molar ratio of methanol to air in the methanol catalytic combustion reaction was fixed at 0.14. The methanol catalytic combustion reaction performance of the microreactor with the different catalytic combustion reaction supports was studied under 0.26mL/min, 0.78mL/min and 1.3mL/min injection rates of liquid methanol, respectively. Moreover, a small amount (0.5 g) of Cu/Zn/Al/Zr catalyst was loaded on the 110 PPI copper foam of the self-thermal methanol steam reforming microreactor. The reaction performance of the self-thermal methanol steam reforming microreactor with different catalytic combustion reaction supports was investigated under different self-thermal temperatures with 10 mL/h injection rate of methanol-water mixture.

3. Results and discussion

3.1 Methanol catalytic combustion reaction performance of microreactor

Fig.6 shows an optical image of methanol combustion for porous reaction supports with different structures. The brightness of the flame in the reaction chamber plate for combustion increases with increasing methanol and air flow rates. Moreover, compared with A-type and B-type catalytic combustion reaction supports, the brightness differences in flames at different locations on the reaction chamber for combustion with C-type support were little. Following an increase in methanol and air flow rates, the amount of reaction gas for methanol catalytic combustion increased. Consequently, more exothermic quantity was generated from the methanol catalytic combustion reaction and the more flames in the reaction chamber for combustion were arose. In the C-type support, the front of the reaction chamber plate for combustion had less catalyst particles than the back of the reaction chamber plate to prevent overreaction of reaction gas in the front of the reaction chamber plate and reduce the temperature differences between various locations on the reaction chamber plate[15].

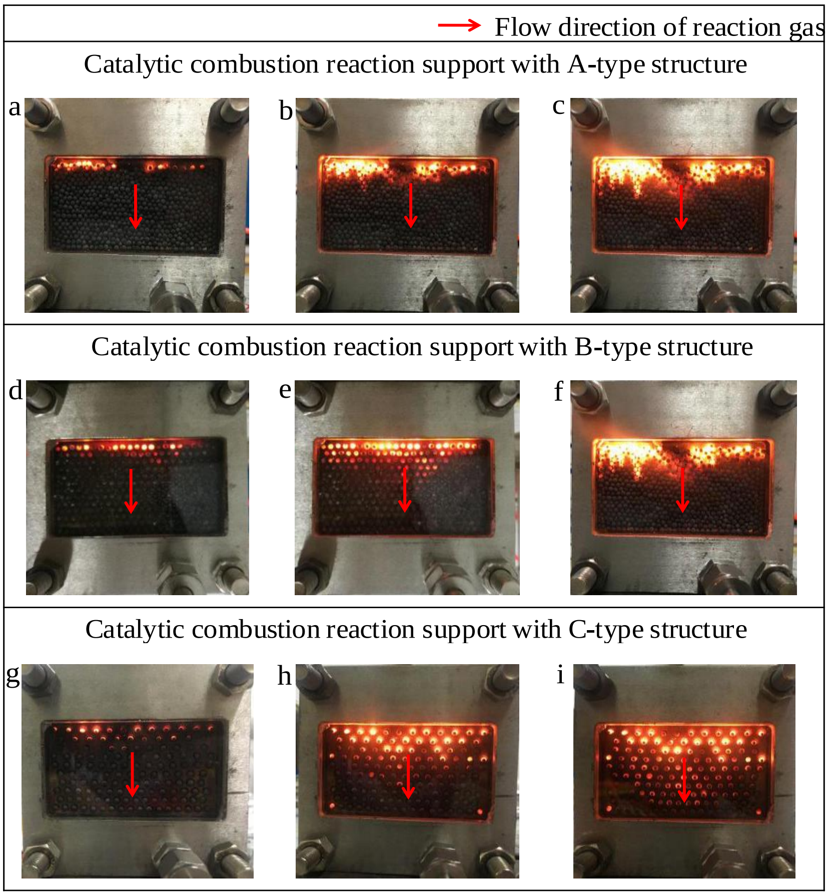

Fig.6. Optical image of methanol combustion for porous reaction supports with different structures. Catalytic combustion reaction support with A-type structure under different injection rates of methanol: (a) 0.26 mL/min, (b) 0.78 mL/min and (c) 1.3 mL/min. The next three correspond to catalytic combustion reaction support with B-type structure under different injection rates of methanol: (d) 0.26 mL/min, (e) 0.78 mL/min and (f) 1.3 mL/min. Finally, the catalytic combustion reaction support with C-type structure under different injection rates of methanol: (g) 0.26 mL/min, (h) 0.78 mL/min and (i) 1.3 mL/min.

Fig.7 shows the infrared thermography of methanol combustion for porous reaction supports with different structures. Compared with A-type and B-type catalytic combustion reaction supports, the thermal distribution region with relatively high temperature for C-type support was closer to the centre of the reaction chamber for combustion. Moreover, the thermal distribution region with a relatively high temperature was larger. It was shown that the thermal distribution of the reaction chamber plate for combustion can be controlled by changing the catalyst distribution in the reaction chamber plate.

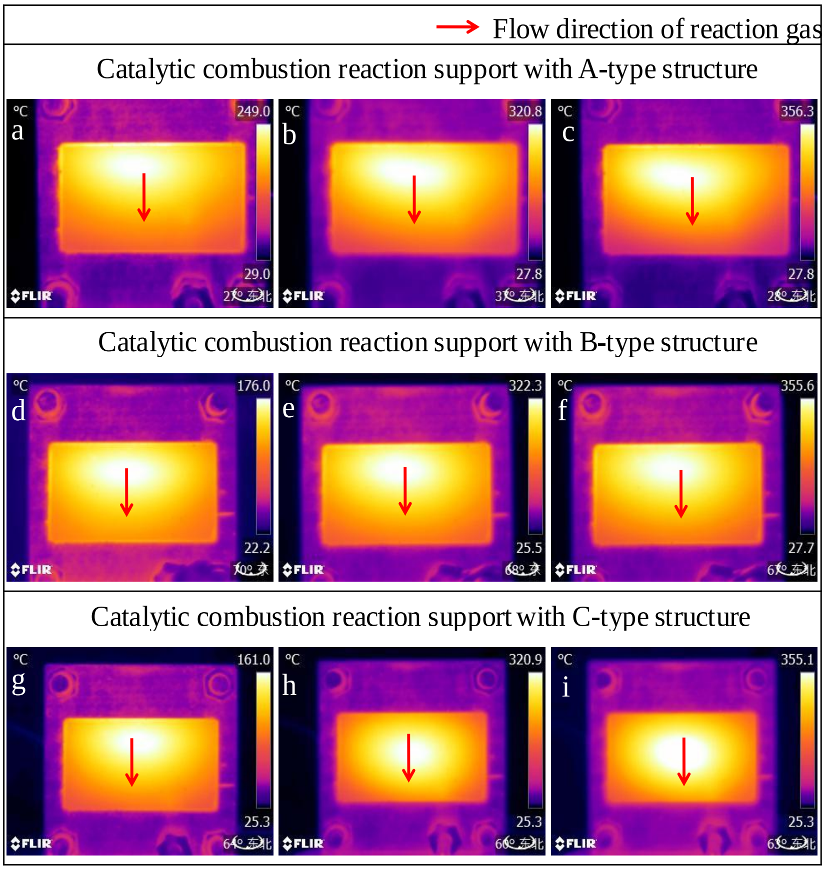

Fig.7. Infrared thermography of methanol combustion for porous reaction supports with different structures. Catalytic combustion reaction support with A-type structure under different injection rates of methanol: (a) 0.26 mL/min, (b) 0.78 mL/min and (c) 1.3 mL/min. Then, in the B-type structure under different injection rates of methanol: (d) 0.26 mL/min, (e) 0.78 mL/min and (f) 1.3 mL/min. Finally, in the C-type structure under different injection rates of methanol are shown: (g) 0.26 mL/min, (h) 0.78 mL/min and (i) 1.3 mL/min.

Fig.8 shows the maximum temperature differences of thermal distribution on the reaction chamber plate for combustion with different catalytic combustion reaction supports. Compared with A-type and B-type supports, the maximum temperature difference of thermal distribution ($\triangle T_{max}$) between nine locations of the reaction chamber plate for combustion with C-type support was lower under different injection rates. The values of $\triangle T_{max}$ of A-type, B-type and C-type support structures were 47.2℃, 35.3℃ and 22.8℃, respectively. Compared with A-type structure, the $\triangle T_{max}$ of C-type support was decreased by 24.4℃. These were compared to examine the fact that the temperature difference of thermal distribution on the reaction chamber plate for combustion can be decreased using the C-type catalytic combustion reaction support. It can be concluded that the gradient gap distribution of Pt/Al2O3 catalyst particles on the 110 PPI copper foam was beneficial for decreasing the △Tmax of thermal distribution on the reaction chamber plate for combustion.

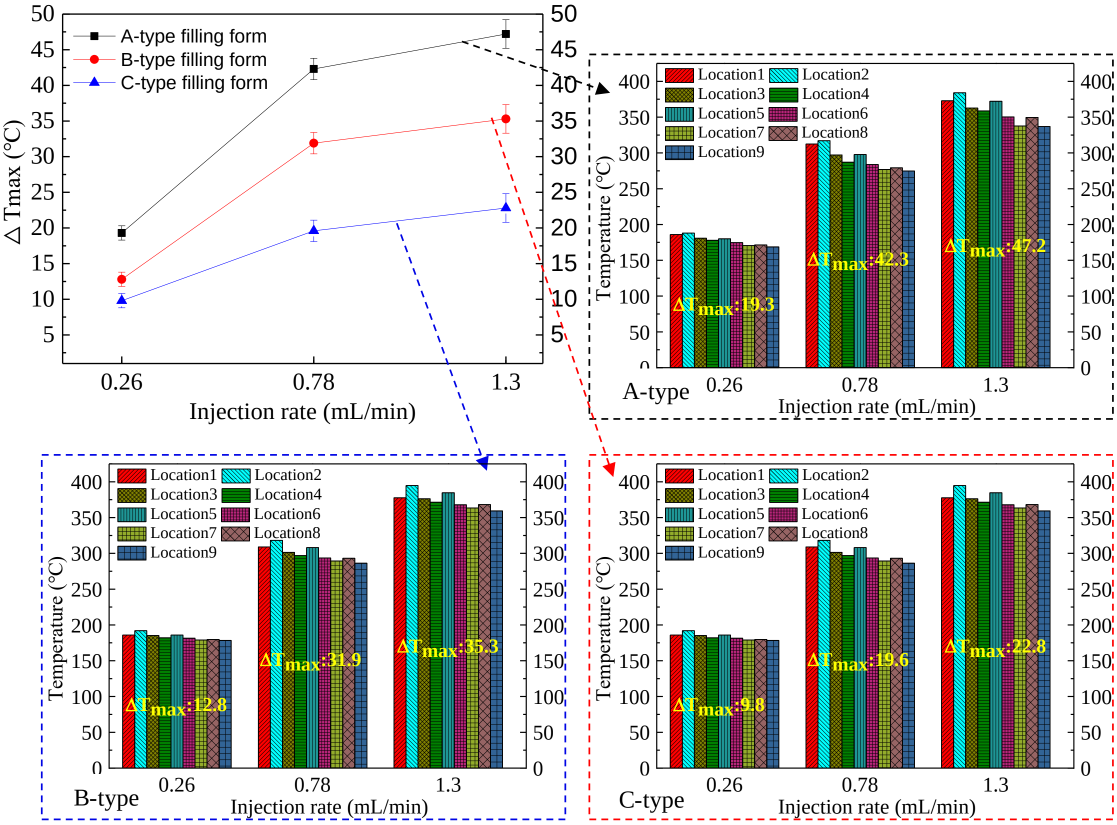

Fig.8. Maximum temperature differences of thermal distribution on the reaction chamber plate for combustion with different catalytic combustion reaction supports

3.2 Reaction performance of self-thermal methanol steam reforming microreactor

Fig.9 shows the reaction performance in hydrogen production of the self-thermal methanol steam reforming microreactor with different catalytic combustion reaction supports under different self-thermal temperatures. By increasing the self-thermal temperature, the methanol steam reforming reaction performance was increased; moreover, the methanol steam reforming reaction performance gap between the microreactors with different catalytic combustion reaction supports widened. Compared with A-type and B-type reaction supports, the reaction chamber plate for combustion with C-type support exhibited a better methanol steam reforming reaction performance. Especially, compared with A-type, methanol conversation of C-type support was increased by 15.2%, the H_2 flow rate was increased by 15.2% under 10 mL/h methanol-water mixture injection rate and 340 ℃ reaction temperature. Meanwhile, the CO selectivity was decreased by 4.1%. It was shown that Compared with the high value of $\triangle$Tmax of thermal distribution on the reaction chamber plate for combustion, the smaller value was beneficial for increasing the methanol steam reforming reaction performance of self-thermal microreactor. Compared with A-type and B-type reaction support, the temperature difference of thermal distribution on the reaction chamber plate with C-type support for combustion was smaller. Accordingly, the temperature difference of thermal distribution on the reaction chamber plate for reforming was smaller. Thus the problem of local catalyst deactivation caused by local high temperature will not occur in the reaction chamber plate for reforming[26-29].

In this way, the overall catalytic performance of the catalyst in the reaction chamber plate for reforming will be better[13]. Therefore, the self-thermal microreactor exhibited a better methanol steam reforming reaction performance in hydrogen production.

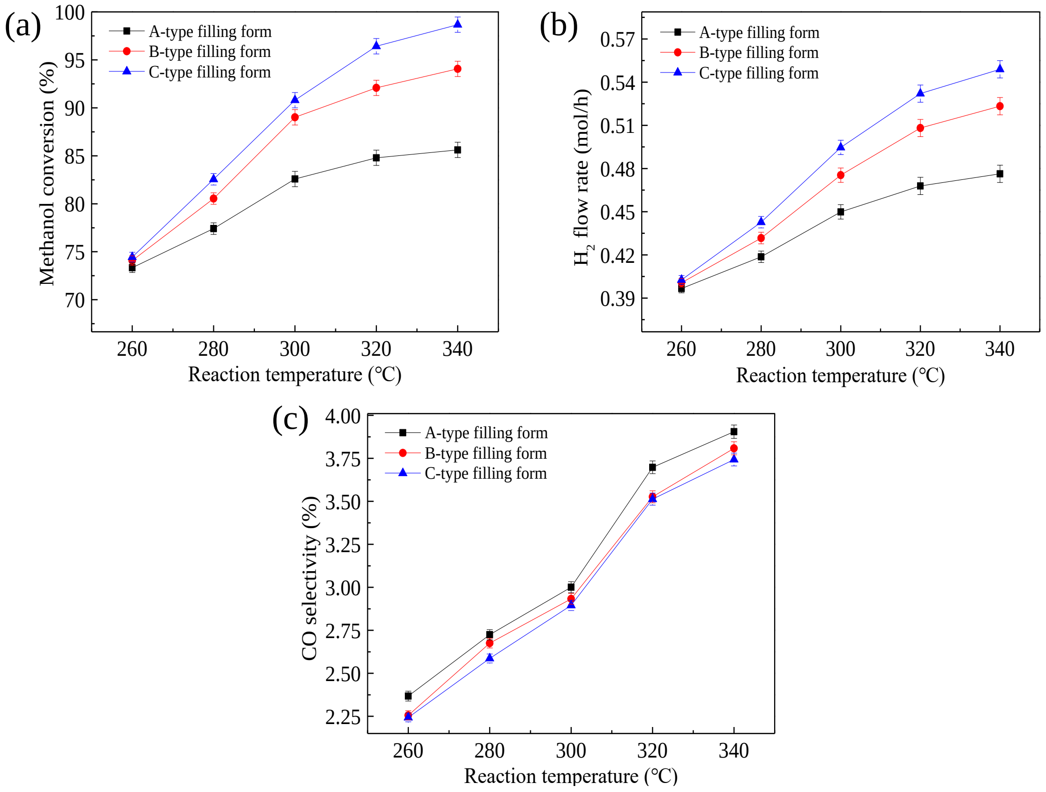

Fig.9. Reaction performance in hydrogen production of the self-thermal methanol steam reforming microreactor with different catalytic combustion reaction supports under different self-thermal temperatures: (a) Methanol conversion, (b) H_2 flow rate, (c) CO selectivity.

4. Conclusions

Combined with the previous research works of the methanol steam reforming microreactor, a methanol catalytic combustion microreactor, a self-thermal methanol steam reforming microreactor for hydrogen production and the corresponding testing systems were developed. Moreover, the catalytic combustion reaction supports with different structures were designed and manufactured. Furthermore, the related experiments were done. It was found that the developed self-thermal microreactor for hydrogen production can replace traditional electrical heating mode by using methanol catalytic combustion as the heat-supply of the methanol steam reforming reaction. Moreover, compared with A-type support, the $\triangle T_{max}$ of C-type support was decreased by 24.4℃. The thermal distribution of the reaction chamber for combustion can be controlled by changing the catalyst distribution in the reaction chamber plate. Compared with A-type support, the methanol conversation and H_2 flow rate of the self-thermal microreactor with C-type porous reaction support were increased by 15.2% under 10 mL/h methanol-water mixture injection rate and 340 ℃ self-thermal. Meanwhile, the CO selectivity was decreased by 4.1%. It can be concluded that the gradient gap distribution of Pt/Al_2O_3 catalyst particles on the 110 PPI copper foam was beneficial for decreasing the $\triangle T_{max}$ of thermal distribution on the reaction chamber plate for combustion. Compared with the high value of $\triangle T_{max}$ of thermal distribution on the reaction chamber plate for combustion, the smaller value was beneficial for increasing the methanol steam reforming reaction performance of self-thermal microreactor.

Acknowledgments

This work was supported by the National Natural Science Foundation of China (Nos.51975496 and 51922092), the Natural Science Foundation of Fujian Province of China (No.2017J06015) and Guangdong Natural Science Funds for Distinguished Young Scholars (No.2016A030306032). Moreover, the supports from Xiamen University and the Fundamental Research Fund for Central Universities

(No.20720180076) are also acknowledged.

References

[1] Dincer I, Acar C. Review and evaluation of hydrogen production methods for better sustainability. Int J Hydrogen Energy. 2015;34:11094-111.

[2] Wang F, Cao YD, Wang GQ. Thermoelectric generation coupling methanol steam reforming characteristic in microreactor. Energy. 2015;80:642-53.

[3] Gholami A, Pourfayaz F, Hajinezhad A, Mohadesi M. Biodiesel production from Norouzak (Salvia leriifolia) oil using choline hydroxide catalyst in a microchannel reactor. Renew Energ. 2019;136:993-1001.

[4] Tian JS. Ke YZ, Kong GG, Tan MW, Wang Y, Lin JD, et al. A novel structured PdZnAl/Cu fiber catalyst for methanol steam reforming in microreactor. Renew Energ. 2017;113:30-42.

[5] Mei DQ, Qian M, Yao ZH, Liu BH, Lou XY, Chen ZC. Effects of structural parameters on the performance of a micro-reactor with micro-pin-fin arrays (MPFAR) for hydrogen production. Int J Hydrogen Energy. 2012;37:17817-27.

[6] Zhou W, Yu W, Ke YZ, Liu YX, Wan SL, Lin JD. Size effect and series-parallel integration design of laminated methanol steam reforming microreactor for hydrogen production. Int J Hydrogen Energy. 2018;43:19396-404.

[7] Zhou W, Ke YZ, Wang QH, Wan SL, Lin JD, Zhang JP, et al. Development of cylindrical laminated methanol steam reforming microreactor with cascading metal foams as catalyst support. Fuel. 2017;191:46-53.

[8] Rath R, Kumar P, Mohanty S, Nayak, SK. Recent advances, unsolved deficiencies, and future perspectives of hydrogen fuel cells in transportation and portable sectors. Int J Energ Res. 2019;15:8931-55.

[9] Gu XG, Taylor RA, Li Q, Scott JA, Rosengarten G. Thermal analysis of a micro solar thermal collector designed for methanol reforming. Solar Energy. 2015;113:189-98.

[10] Tanaka SJ, Chang KS, Min KB, Satoh D, Yoshida K, Esashi M. MEMS-based

components of a miniature fuel cell/fuel reformer system. Chem Eng J. 2004;101:143-49.

[11] Chein RY, Chen YC, Chen JY, Chung JN. Design and test of a miniature hydrogen production reactor integrated with heat supply, fuel vaporization, methanol-steam reforming and carbon monoxide removal unit. Int J Hydrogen Energy. 2012;37:6562-71.

[12] Hsueh CY, Chu HS, Yan WM, Chen CH. Numerical study of heat and mass transfer in a plate methanol steam micro reformer with methanol catalytic combustor. Int J Hydrogen Energy. 2010;35:6227-38.

[13] Herdem MS, Mundhwa M, Farhad S, Hamdullahpur F. Multiphysics modeling and heat distribution study in a catalytic microchannel methanol steam reformer. Energy Fuel. 2018;32:7220-34.

[14] Wang F, Wang GQ. Performance and cold spot effect of methanol steam reforming for hydrogen production in micro-reactor. Int J Hydrogen Energy. 2016;41:16835-41.

[15] Zheng TQ, Zhou W, Yu W, Ke YZ, Liu YX, Liu RL, Kwan SH. Methanol steam reforming performance optimisation of cylindrical microreactor for hydrogen production utilising error backpropagation and genetic algorithm. Chem Eng J. 2019; 357:641-54.

[16] Chen WH, Shen CT, Lin BJ, Liu SC. Hydrogen production from methanol partial oxidation over Pt/Al_2O_3 catalyst with low Pt content. Energy. 2015;88:399-407.

[17] Alvarez-Galvan MC, Navarro RM, Rosa F, Briceño Y, Ridao MA, Fierro JLG. Hydrogen production for fuel cell by oxidative reforming of diesel surrogate: Influence of ceria and/or lanthana over the activity of Pt/Al_2O_3 catalysts. Fuel. 2008;87:2502-11.

[18] Parmar RD, Kundu A, Thurgood C, Peppley BA, Karan K. Kinetic studies of the autothermal reforming of tetradecane over Pt/Al_2O_3 catalyst in a fixed-bed reactor. Fuel. 2010;89:1212-20.

[19] Luo YJ, Xiao YH, Cai GH, Zheng Y, Wei K. Performance of $Ce_{0.25}Zr_{0.75}O_2$ promoted Pd/Ag/c-Al_2O_3 catalysts for low-temperature methanol oxidation. Fuel.

2012;93:533-38.

[20] Fu BR, Ting YC, Lee CF, Huang YJ, Su YC, Tseng FG, Pan C. Real-time monitoring of a micro reformer integrated with a microchannel heat exchanger by infrared thermography and high-speed flow images. Int J Hydrogen Energy. 2016;41:18610-20.

[21] EI-Amiri A, Saifi A, Elhassnaoui A, Obbadi A, Errami Y, Sahnoun S. Control of solid oxide fuel cells damage using infrared thermography. Int J Hydrogen Energy. 2020;45:11695-703.

[22] Park GG, Seo DJ, Park SH, Yoon YG, Kim CS, Yoon WL. Development of microchannel methanol steam reformer. Chem Eng J. 2004;101:87-92.

[23] Yu H, Chen H, Pan M, Tang Y, Zeng K, Peng F, et al. Effect of the metal foam materials on the performance of methanol steam micro-reformer for fuel cells. Appl Catal A-Gen. 2007;327:106-13.

[24] Mei DQ, Feng YB, Qian M, Chen ZC. An innovative micro-channel catalyst support with a micro-porous surface for hydrogen production via methanol steam reforming. Int J Hydrogen Energy. 2016;41:2268-77.

[25] Zheng TQ, Zhou W, Geng D, Li YY, Liu YX, Zhang CY. Methanol steam reforming microreactor with novel 3D-Printed porous stainless steel support as catalyst support. Int J Hydrogen Energy. 2020;45:14006-16.

[26] Twigg MV, Spencer MS. Deactivation of supported copper metal catalysts for hydrogenation reactions. Appl Catal A-Gen. 2001; 212:161-74.

[27] Ajamein H, Haghighi M, Shokrani R, Abdollahifar M. On the solution combustion synthesis of copper based nanocatalysts for steam methanol reforming: Effect of precursor, ultrasound irradiation and urea/nitrate ratio. J Mol Catal A-Chem. 2016;421:222-34.

[28] Minaei S, Haghighi M, Jodeiri N, Ajamein H, Abdollahifar M. Urea-nitrates combustion preparation of CeO_2-promoted $CuO/ZnO/Al_2O_3$ nanocatalyst for fuel cell grade hydrogen production via methanol steam reforming. Adv Powder Technol. 2017;28:842-53.

[29] Zhu QF, Zhang QC, Wen LX. Anti-sintering silica-coating CuZnAlZr catalyst for

methanol synthesis from CO hydrogenation. Fuel Process Technol. 2017;156:280-89.